THE JOURNAL OF PHYSICAL CHEMISTRY C

Article

pubs.acs.org/JPCC

Anatase Nanotubes as an Electrode Material for Lithium-Ion Batteries

G. S. Zakharova,[†] C. Jähne,[§] A. Popa,[‡] Ch. Täschner,[‡] Th. Gemming,[‡] A. Leonhardt,[‡] B. Büchner,[‡] and R. Klingeler*[,§]

[†]Institute of Solid State Chemistry, Ural Division, Russian Academy of Sciences, Pervomaiskaya ul. 91, Yekaterinburg, 620990 Russia

[‡]Leibniz Institut für Festkörper- und Werkstoffforschung IFW Dresden, Helmholtzstrasse 20, 01069 Dresden, Germany

[§]Kirchhoff Institute for Physics, INF 227, University of Heidelberg, 69120 Heidelberg, Germany

ABSTRACT: Anatase TiO_2 nanotubes were synthesized via the hydrothermal method followed by annealing at 500 °C in argon for 1 h. The phase structure, morphology, and composition were investigated in detail by means of X-ray diffraction, scanning and high-resolution transmission electron microscopy, infrared spectroscopy, and thermal analysis. The material consists of nanotubes with diameter of 10−15 nm and lengths of several hundred nanometers. The electrochemical properties were investigated by cyclic voltammetry and galvanostatic cycling. The data imply a first cycle irreversible capacity of 385 mAh/g, and capacities of 307 and 265 mAh/g after the second and 50th cycle, respectively, at C/10. The Coulombic efficiency of about 99% after cycle 50 implies excellent cycling stability. Hence anatase TiO_2 nanotubes evidence great potential for usage in high-power lithium-ion batteries.

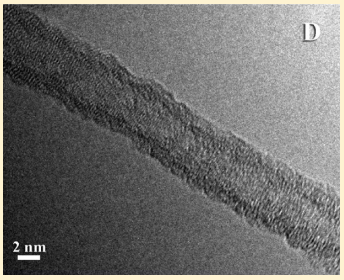

1. INTRODUCTION

During the past decade, transition metal oxide nanomaterials have received a lot of attention because of the wide field of potential applications like sensors, solar cells, and battery materials.[1−3] From a fundamental point of view, this potential arises not only from the mere size reduction but from fundamentally novel properties appearing upon size reduction which may yield new applications for well-known bulk materials. One of the most studied and applied oxide nanomaterials is the class of titanium oxides that is used for a variety of applications such as photocatalysis, hydrogen storage, and sensing.[4,5] High surface area and reduced ionic or/and electronic diffusion lengths as well as less tendency to structural changes compared to the bulk form render nanoscaled materials beneficial for electrochemical energy storage. Indeed, titanium oxides are good candidates for an anode material in lithium-ion batteries because of high safety, good capacity retention, and low self-discharge.[6] In addition, TiO_2 is characterized by excellent cyclability, chemical stability, and negligible toxicity while it is relatively simple to prepare.[7] In particular, its layered structure is supposed to facilitate the diffusion of the Li^+ ions when being used as an electrode in lithium-ion batteries.[8] A main aspect concerning using TiO_2 as electrode material is its electrochemical potential in the range of 1.5−1.7 V vs Li/Li^+ depending on the actual structural modification. The low potential where most of the Li intercalation takes place renders TiO_2 a powerful candidate for electrodes in lithium-ion batteries. In fact, the high working potential in comparison to carbon yields lower overall cell voltages and prevents agglomeration of lithium at the negative electrode, thereby enhancing safety and cell lifetime while high energy density applications are excluded.

Due to high aspect ratio and porous morphology, elongated TiO_2 nanostructures such as rods or tubes allow efficient transport of lithium ions and a high charge/discharge capacity (about 300 $mAhg^{-1}$).[9] From the various titanium oxide phases, in particular, anatase, rutile, and TiO_2(B), have been extensively investigated regarding their electrochemical properties.[6,10] The synthesis methods as well as the precursors chosen for preparing TiO_2 play a very important role. Depending on these parameters, the finite size of TiO_2 can be tailored, and from here different capacity values are found for TiO_2 with different particle size.[11] Anatase TiO_2 presents highly interesting properties for possible application in lithium-ion batteries. Its tetragonal structure (space group $I4_1/amd$) consists of edge-sharing distorted TiO_6 octahedra forming infinite planar double chains. Between the octahedra there are vacant octahedral and tetrahedral sites that may be occupied by Li through lithiation during electrochemical treatment.[7] Here, we report the electrochemical properties of anatase TiO_2 nanotubes which were synthesized by hydrothermal treatment in NaOH medium and annealed at 500 °C in argon for 1 h. The material shows extraordinary specific capacity as well as very good cycling stability and capacity retention, thereby evidencing its potential for applications in lithium-ion batteries, which are optimized regarding stability, lifetime, and safety issues.

Received: July 20, 2011
Revised: April 2, 2012
Published: April 2, 2012

2. EXPERIMENTAL SECTION

Anatase TiO_2 nanotubes have been prepared according a protocol for anatase nanoparticle synthesis described by Peng et al.,[12] with a NaOH aqueous solution as first reported by Kasuga et al.[13] A typical synthetic procedure was as follows: 0.5 g of anatase-type TiO_2 powder was mixed with 12 mL 10 M NaOH aqueous solution using the ultrasonic bath for 30 min. Then the suspension was transferred into a Teflon-lined stainless steel autoclave (45 mL capacity), kept at 150 °C for 48 h, and finally cooled to room temperature naturally. The precipitate was filtered off and washed with 0.1 M HCl and water to get the neutral medium. The precipitate was dried at room temperature in air.

The product was characterized by X-ray diffraction (XRD; DRON-2, Cu Kα radiation, λ = 1.5418 Å). The morphology of the powder was determined by means of a FEI Tecnai F30 high-resolution transmission electron microscope (HRTEM) and a NanoSEM (FEI) scanning electron microscope (SEM). Elemental analysis was carried out using an energy-dispersive X-ray spectrometer (EDX) by preliminary plasma sputtering of a gold film on the samples in argon atmosphere. Fourier transform infrared (FT-IR) spectra were recorded on a Perkin-Elmer Fourier-transform spectrometer with a resolution of 0.5 cm^{-1}. Thermal analysis of TiO_2 nanotubes was performed on a SDT Q600 from TA Instruments, which allows simultaneous measurements of differential scanning calorimetry (DSC) and thermogravimetric analysis (TGA). The powdery sample was heated with a rate of 20 K/min from room temperature up to 800 °C in nitrogen atmosphere. For the electrochemical studies, electrode materials have been prepared from a mixture of TiO_2 nanotubes annealed at 500 °C, 10 wt % of Carbon SP (Timcal, LTd, Bodio, Switzerland) and 10 wt % of polyvinylidene fluoride (PVDF) binder (Solexis, Tavaux Cedex, France). This mixture was then soaked with *N*-methyl-2-pyrrolidone (NMP; Aldrich) resulting in a slurry. Aluminum grid pellets were used as electrode support (approximately 10 mm in diameter). Before the electrodes were used, they were dried in the oven for 12 h. A mixture containing approximately 4 mg of TiO_2 nanotubes was put on the aluminum grid, placed in two-electrode Swagelok-like cells, and pressed. This procedure yields an electrode density as calculated from the total amount of mixture per electrode area of about 5 mg TiO_2/cm^2. The cells were assembled inside the glovebox under argon atmosphere (O_2 and H_2O level <2 ppm). In the two-electrode cell, lithium metal was used as a negative electrode, and TiO_2 nanotubes were used as positive electrode. The two parts were separated by two sheets of Whatman borosilicate glass fiber and soaked in electrolyte in order to maintain good ionic conductivity and physical separation of the two electrodes.[14] The used electrolyte was 1 M solution of $LiPF_6$ salt in ethylene carbonate (EC)/dimethyl carbonate (DMC) in a weight ratio of 1:1 (Ferro Corporation, Cleveland, OH). Cyclic voltammetry and galvanostatic measurements were performed using a VMP multichannel controller (Princeton Applied Research, Illingen, Germany). The experiments were performed in a heating chamber at a temperature of T = 25 °C.

3. MORPHOLOGY AND CHARACTERIZATION

XRD patterns of as-prepared TiO_2 nanotubes and TiO_2 nanotubes after annealing at 400 and 500 °C in Ar for 1 h, respectively, are shown in Figure 1. All of the diffraction peaks

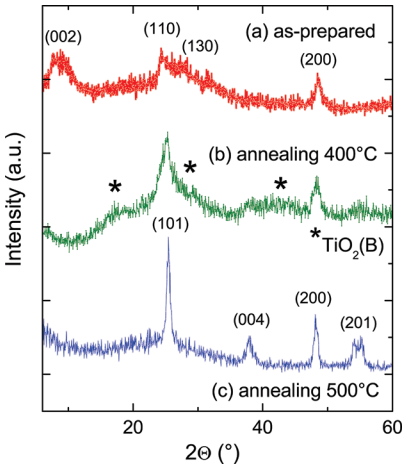

Figure 1. XRD patterns of (a) as-prepared TiO_2 nanotubes, (b) nanotubes after annealing at 400 °C, and (c) nanotubes after annealing at 500 °C in Ar for 1 h. Peak indices in panels a and c refer to the anatase phase. The reflections corresponding to the TiO_2(B) phase are marked by asterisks in panel b.

of the as-prepared TiO_2 nanotubes (Figure 1a) can be indexed to a lepidocrocite-type titanate phase $H_xTi_{2-x/4}\square_{x/4}O_4{\cdot}H_2O$.[15] Annealing the as-prepared TiO_2 nanotubes at 400 °C leads to the formation of a mixed TiO_2 anatase and TiO_2(B) phase (cf. Figure 1b).[16] When the temperature was increased to 500 °C, only the anatase phase was found (Figure 1c), while superstructure reflections related to the TiO_2(B) phase are not observed. In addition, the anatase superstructure peaks of the sample annealed at 500 °C exhibit larger heights and smaller full width at half-maximum as compared to the one annealed at 400 °C. The latter observation indicates that the mean crystallite size increases with treatment temperature.

Morphology, size, and purity of the titanium dioxide before and after calcinations at 500 °C in Ar were studied by means of SEM and HRTEM imaging (Figure 2). Figure 2a shows that

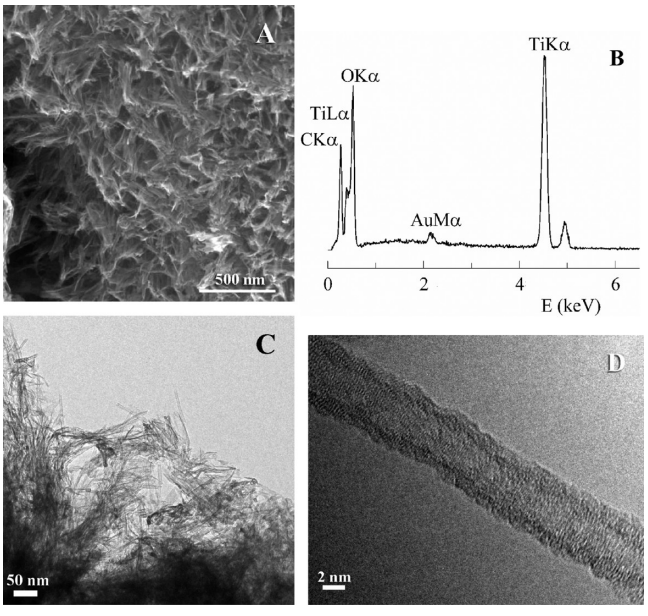

Figure 2. (a) SEM image of as-prepared TiO_2 nanotubes; (b,c) HRTEM images and (d) EDX pattern of TiO_2 nanotubes after annealing at 500 °C in Ar for 1 h (see the text).

dx.doi.org/10.1021/jp300955r | J. Phys. Chem. C 2012, 116, 8714−8720

the as-prepared nanotubes are several hundred nanometers in length. After annealing, only slight aggregation is found, and the tubular morphology of the product is preserved (Figure 2b). This is particularly highlighted by Figure 2c, where HRTEM imaging clearly shows the tubular morphology of the final product. The mean size of the nanotubes is, however, affected by the thermal treatment as already indicated by the narrowing of the XRD peaks. The results of EDX analysis (Figure 2d) shows that the nanotubes contain the elements Ti and O. Additional peaks are due to the carbon tape used for fixing of the samples and the gold film covering the samples, respectively. In particular, there is no trace of sodium in the final product. To summarize our TEM studies, after appropriate postsynthesis treatment, the procedure yields pure and rather uniform anatase TiO_2 nanotubes with around 4−6 nm inner diameter and 10−15 nm outer diameter. We note that our results somehow contradict the data in ref 17, which indicate the transformation of protonated TiO_2 nanotubes and formation of anatase with rod-like morphology after annealing in air at temperatures higher than 400 °C.

A fair estimate of the nanotubes' diameters can be extracted from the width of the XRD diffraction peaks, too, providing an independent estimate of the particle size. According to the Scherrer equation, the mean particle size D_{XRD} amounts to[18]

$$D_{XRD} = \frac{0.93\lambda}{\Delta 2\theta_{(hkl)} \cos \theta_{(hkl)}}$$

Here, λ is the wavelength of the applied Cu Kα radiation, $\Delta 2\theta_{(hkl)}$ is the full width at half-maximum of the diffraction peak, and $\theta_{(hkl)}$ is the Bragg angle. For the material post-treated at 500 °C, the analysis of the (1 0 1), (0 0 4), and (2 0 0) peaks yields $D_{101} \approx 15$ nm, $D_{004} \approx 8$ nm, and $D_{200} \approx 14$ nm, respectively. One might speculate, however, that the large width of the (0 0 4) might be due to merging with the nearby (1 0 3) and (1 1 2) peaks, so that D_{004} is questionable and should be disregarded. In contrast, the (2 0 0) diffraction peak is clearly visible in all three samples and well separated from other peaks, either originating from anatase or competing phases. Analyzing its width hence allows estimating size changes of the nanostructures upon postsynthesis treatment. The as-prepared material and the material annealed at 400 °C exhibit a similar width of the peak, and hence similar mean particle sizes of $D_{200} \approx 8.9$ and 8.3 nm, respectively, are obtained by applying Scherrer's equation. By contrast, annealing at 500 °C not only affects the phase but also yields a considerable size increase as we find $D_{200} \approx 14$ nm.

In Figure 3a, the thermal and gravimetric analysis curves (DSC and TG) for TiO_2 nanotubes annealed at 500 °C are shown. According to the TG data, there is an integrated weight loss of 3.9% upon heating up to 800 °C. The weight of the sample decreases continuously up to about 500 °C. The DSC data demonstrate an endothermic effect at around 81 °C, which can be straightforwardly attributed to dehydration. The loss of weight hence indicates an initial composition of $TiO_2 \cdot 0.18H_2O$ nanotubes. The presence of interstitial water in the annealed TiO_2 nanotubes is indeed confirmed by the FT-IR spectra displayed in Figure 3b. At small wave numbers, there are several features that can be associated with vibrations of TiO_2.[19] To be specific, the pronounced absorption below 850 cm^{-1} is due to lattice vibrations of TiO_2, while the weak band at 975 cm^{-1} corresponds to asymmetric stretching vibrations of the octahedral $[TiO_6]$ groups. Another clear feature appears as a

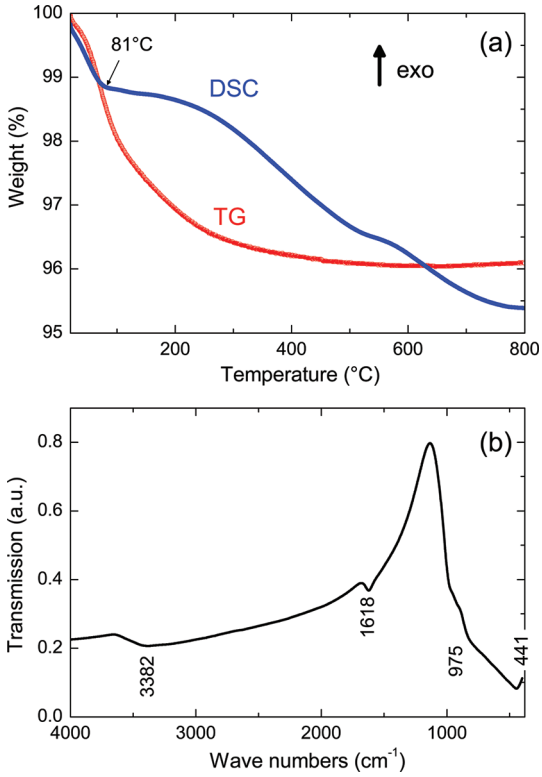

Figure 3. (a) DSC and TG scans (5.231 mg) and (b) FTIR spectra of TiO_2 nanotubes after thermal annealing at 500 °C in argon for 1 h.

broad peak from 3000 to 3600 cm^{-1} with the center around 3382 cm^{-1}. This peak can be assigned to the stretching vibration of the hydrogen-bonded OH groups of the adsorbed water. Further support to this scenario is given by the absorption peak at 1618 cm^{-1}, which is associated with the bending vibration of adsorbed H_2O molecules.

The FT-IR data hence confirm the presence of water in TiO_2 nanotubes even after annealing at 500 °C in Ar. Indeed, it is well-known that TiO_2 may exhibit hydrophilic surface enriched with superficial hydroxyl groups. These surface hydroxyl groups can be preserved even after high-temperature treatment up to 600 °C.[20] Perhaps the presence of the water molecules inside the TiO_2 nanotubes allows preserving the tubular morphology. This may explain the discrepancy of our results, i.e., preservation of tubular morphology upon calcination at 500 °C, compared to previous studies that imply the formation of rod-like structures under these conditions.[17]

4. CYCLIC VOLTAMMETRY AND GALVANOSTATIC CYCLING

In Figure 4, cyclic voltammograms (CVs) of the annealed TiO_2 nanotubes are shown recorded at a scan rate of 0.05 mV/s in the potential range of 4.2−1 V vs Li/Li^+. The figure shows four consecutive cycles performed on a fresh cell with open cell voltage of 3.06 V vs Li/Li^+. The main features are pronounced cathodic and anodic peaks at 1.70 and 1.99 V, respectively, which are associated with electrolytic lithium insertion into and extraction from the anatase structure, according to the schematic reaction

$$TiO_2 + xLi^+ + xe^- \leftrightarrow Li_xTiO_2$$

In the first cycle, the hysteresis between the main insertion and extraction processes amounts to 0.28 V vs Li/Li^+, which

dx.doi.org/10.1021/jp300955r | J. Phys. Chem. C 2012, 116, 8714−8720

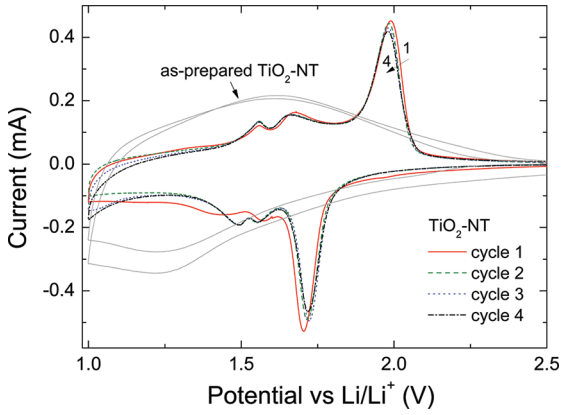

Figure 4. CV for (annealed) TiO_2 nanotubes performed with a scan rate of 0.05 mV/s. For comparison, gray lines display the first two cycles of the as-prepared material.

slightly reduces to ~0.26 V in the fourth cycle. In addition to the main peaks, there are additional features that show up in both the reduction and oxidation regimes. Cathodic minor peaks appear at 1.57 and 1.44 V, while a bit more distinguished anodic ones are visible at 1.55 and 1.67 V. Starting with the second cycle, the cathodic minor peaks become more pronounced, too, and shift to 1.55 V and 1.49 V, respectively. In the following cycles, their position and intensity remain unchanged compared to those of the second cycle. On the anodic side, there is much less modification upon cycling. The ratio of the main anodic to cathodic peak height is almost equal. Both observations, i.e., minimal changes in the shape of CVs during cycling and the constant ratio of the peak heights, indicate the reversibility of the lithium-ion intercalation/deintercalation process from the second cycle onward. For comparison, the first two CVs obtained for the as-prepared material are presented, too. The data show that there are no well-pronounced cathodic or anodic peaks.

Galvanostatic discharge/charge profiles of the TiO_2 nanotube electrode were recorded between cutoff voltages of 3.5 and 1 V vs Li/Li^+, at different scan rates between C/10, corresponding to a current density of 33.5 mA/g, and 2C. The results are shown in Figure 5. First, we discuss the data obtained at C/10. During the initial discharge and charge processes, the capacity of the electrode was 385 mAh/g and 305 mAh/g, respectively.

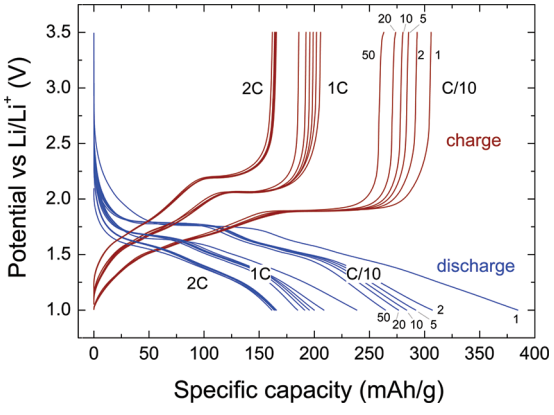

Figure 5. Potential versus specific capacity in Li_xTiO_2 nanotubes obtained from galvanostatic studies. The scans have been performed at different C-rates: 2C, C, and C/10 (33.5 mA/g). For each C-rate, scan numbers 1, 2, 5, 10, 20, and 50 are presented, respectively.

Considering the theoretical capacity of 335 mAh/g, which is associated with the doping level $x = 1$, i.e., $LiTiO_2$,[21] this implies a Li content of about $x = 1.15$, exceeding previously reported values of pure anatase, TiO_2(B), or mixed phases.[11,22,23] In addition, the values indicate that the annealed TiO_2 nanotubes exhibit an irreversible capacity of 79 mAh/g with a reversible capacity of 307 mA h/g in the initial discharge−charge cycle. The irreversibility of about 21% suggests $x = 0.23$ lithium remaining in the material or being consumed in side reactions after the initial cycle.

The voltage profiles provide information on the mechanism of lithium exchange. For all recorded C/10 cycles, the galvanostatic profiles are rather complex and, in particular, display pronounced plateaus at about 1.77 and 1.95 V vs Li/Li^+, respectively, indicating a two-phase structural transition regime. Such behavior is typical for anatase[10] and may be associated with the coexistence of a Li-poor $Li_{0.05}TiO_2$ phase with the anatase space group $I4_1/amd$ and a Li-rich phase $Li_{0.5}TiO_2$ phase exhibiting *Imma*.[24,25] After the initial cycle, there are only modest changes in the data, i.e., neither the complex profile shape nor the specific capacity value is significantly affected by the electrochemical processes. The latter is demonstrated more clearly in Figure 6 where the degradation of the gravimetric

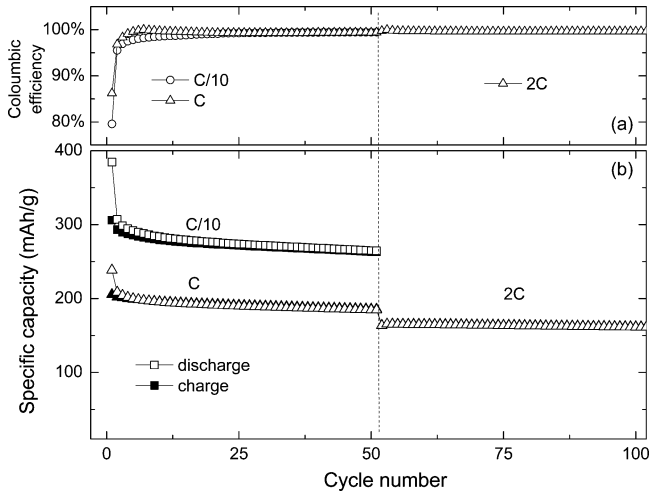

Figure 6. Specific gravimetric capacity (b) and Coulombic efficiency (a) of TiO_2 nanotubes as a function of the cycle number upon cycling under different C-rates.

specific capacity upon discharge/charge cycling is shown. Indeed, starting with the second cycle, the capacity values do not decrease much. After 50 galvanostatic cycles, the discharge capacity stabilizes around 265 mAh/g, which is a high value compared to the 160 mAh/g given by rutile TiO_2[26] or the 190 mAh/g in nanocrystalline anatase TiO_2.[11] To be specific, after 50 cycles, the capacity retention was 69% and 86% between cycles 2 and 50, and 94% between cycles 10 and 50. Note, that these values are superior to similar reports in the literature (e.g., in ref 27). Coulombic efficiency is plotted in Figure 5, too (right ordinate). It amounts to about 80% in the initial cycle, 98% in cycle 5, and ≥99% from cycle 15 onward.

The effect of increasing cycling rates on the voltage profiles is shown in Figure 5, too. For these measurements, a fresh cell was employed so that the first cycle rate 1 C again displays the initial charge/discharge process of electrochemically untreated material. The main effects of increased rates are reduction of the specific charge/discharge capacities and successive

dx.doi.org/10.1021/jp300955r | J. Phys. Chem. C 2012, 116, 8714−8720

suppression of the plateau regime. The latter indicates that the coexistence of the anatase $Li_{0.05}TiO_2$ phase with the *Imma* $Li_{0.5}TiO_2$ phase is strongly suppressed at high cycling rates. The discharge capacity observed under C/10 is reduced to 209 mAh/g (1 C, cycle 2), 166 mAh/g (2 C), and 30 mAh/g (10 C). In general, such reduction of specific capacity is typical for TiO2 electrodes and may be ascribed to the insulating character of the material.[28] The values found in the material at hand are larger than the respective values in TiO_2 brookite nanostructures[10] and in titania (TiO_2) and carbon−titania (C-TiO_2) nanotubes.[28] Indeed, the specific capacities shown in Figure 5 are very similar to the highest ones found in a series of micrometer-sized anatase TiO_2 with different degrees of mesoporosity.[29] In this sense, our synthesis procedure yields optimized material with regard to the interplay of mesoporisity and the formation of a percolation network facilitating Li^+ and electronic conduction.

Post-mortem SEM and HRTEM images (Figure 7) of the cycled material show that tubular structures are still visible after

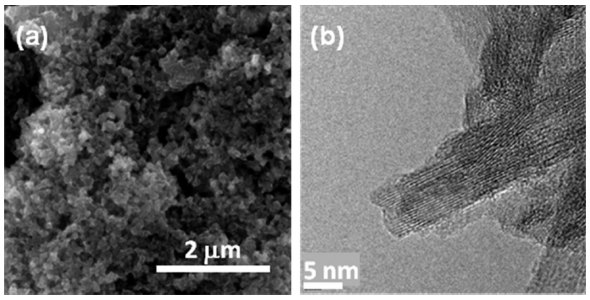

Figure 7. (a) SEM and (b) HRTEM post-mortem images of TiO_2 nanotubes, i.e., after electrode preparation (see the text) and electrochemical cycling.

50 charge/discharge cycles, although there are clear changes as expected due to electrode preparation, which, e.g., includes mixing with 10 wt % of carbon and 10 wt % of PVDF binder. Finally, for comparison, CVs (see Figure 4), galvanostatic charge/discharge profiles, and Coulombic efficiency are shown for the as-prepared material, i.e., without subsequent annealing (Figure 8). The cyclability performed at C/10 is smaller than that of the anatase TiO_2 nanotubes but still reveals fair gravimetric capacities of 169 mAh/g and 159 mAh/g after 10 and 20 cycles, respectively, with associated Coulombic efficiencies of 97 and 98%. For the lepidocrocite-type titanate phase $H_xTi_{2-x/4}\square_{x/4}O_4{\cdot}H_2O$, there is again a large irreversibility of ~35% in the first 2 cycles, which may be associated with the presence of interstitial water and solid electrolyte interface (SEI) formation. Absence of a plateau regime indirectly confirms that the anatase phase is not present in the as-prepared material.

5. DISCUSSION

Upon Li intercalation, the anatase converts to a two-phase product: Li-poor TiO_2 (i.e., $Li_\varepsilon TiO_2$) and Li-rich phase, $Li_{0.5}TiO_2$.[7,24] By inserting lithium into the TiO_2 anatase, it transforms from the original tetragonal host structure into orthorhombic one. In $Li_{0.5}TiO_2$, Ti−Ti bonds formed exclusively along *b* axis sustain the reduction in symmetry but the original anatase framework is only moderately distorted.[24] The Ti−O distances are larger than in pure anatase case. The Li

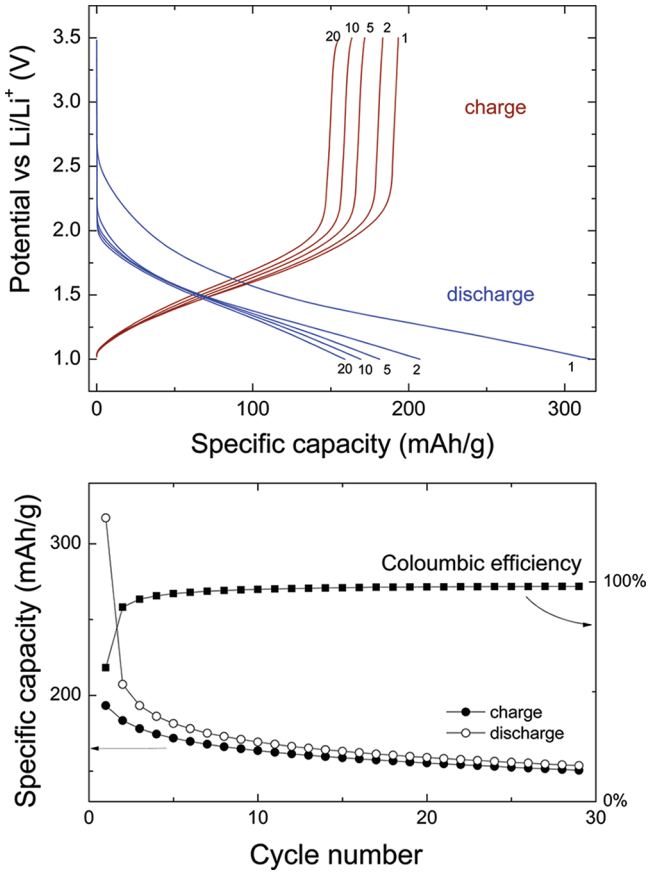

Figure 8. Top: Potential versus specific capacity in as-prepared Li_xTiO_2 nanotubes obtained from galvanostatic studies. The scans have been performed at a rate of C/10. Small Figures (1−20) indicate the respective scan numbers. Bottom: Specific gravimetric capacity and Coulombic efficiency of as-prepared TiO_2 nanotubes as a function of the cycle number.

is known to occupy half of the available interstitial octahedral sites in the distorted ccp TiO_2 anatase host structure.[24]

In pure anatase and rutile TiO_2, single anodic and cathodic peaks corresponding to lithium extraction/insertion are observed. The typical for the anatase lithium intercalation/deintercalation process, manifesting itself in the main cathodic/anodic peaks, is controlled by the diffusion of Li ions in the solid. CV with three pairs of insertion/extraction peaks as seen in Figure 4 have been reported in literature before.[29−31] Various scenarios have been suggested associating these features, e.g., with organized nanotextured anatase made by surfactant templating[30] or with the presence of amorphous titanium oxide.[31] In the case at hand, however, we cannot exclude a tiny amount of TiO_2 (B) in the material, which might survive the 1 h 500 °C calcinations, too less to be detected by our XRD studies. Indeed, a recent study indeed suggests that the minor insertion peaks at 1.55 V and 1.49 V vs Li/Li^+ may be assigned to the TiO_2 (B) phase.[32] One might speculate whether further optimization of the calcinations parameters yields further reduction of the TiO_2 (B) phase. Here, we conclude that the material mainly consists of anatase with a small (<5%) admixture of the TiO_2 (B) phase.

At the beginning of the electrochemical reaction, i.e., before reaching the plateau at ~1.77 V vs Li/Li^+ in the galvanostatic discharge profiles (Figure 5), which indicates the biphasic region, there is an initial monotonous potential decrease. In the

dx.doi.org/10.1021/jp300955r | J. Phys. Chem. C 2012, 116, 8714−8720

first discharge cycle, the monotonous decrease corresponds to approximately 0.2 Li per TiO_2. This value decreases rapidly from the second cycle. Sudant et al. showed that this behavior is associated with a solid solution domain Li_xTiO_2, the extension of which is related to the actual the particle size.[33] The fact that the discharge capacity of the monotonous decrease becomes smaller upon cycling implies the partly irreversibility of lithium exchange in this solid solution domain.

The plateaus at 1.77 and 1.95 V vs Li/Li^+ for discharging and charging, respectively, are in very good agreement with a recent study on anatase TiO_2 nanotubes.[34] The plateau is typical for anatase and indicates the phase equilibrium between $Li_\varepsilon TiO_2$ (with ε the amount of Li inserted in the initial solid solution process) and $Li_{0.5}TiO_2$. At $x = 0.5$, half of Ti^{4+} is converted to Ti^{3+}, a classical Faradaic process due to inserting lithium into the interstitial octahedral sites in anatase TiO_2.[33]

The width of the biphasic region is however smaller than in bulk anatase, indicating that there are less interstitial sites in anatase TiO_2 nanotubes available for Li insertion. A similar observation has been found in ref 11, where effects of size reduction have been suggested to account for the smaller plateau width. To be specific, it is argued that increasing the surface-to-bulk ratio and thereby increasing the proportion of surface and near-to-the surface atoms inevitably decreases the available interstitial octahedral sites for Li insertion in the bulk anatase. Indeed, surface effects are visible in experimental data. The inclined stages at the end and beginning of discharge and charge, respectively, indicate that, after occupying all available interstitial sites, Li ions are inserted into the surface layer under the external force of the electric field.[11] After the initial cycle, these sloped regions do not significantly change, suggesting that the Li surface insertion is highly reversible if trapping in the initial insertion process is completed.

Although it is a general feature of TiO_2 materials to keep some Li trapped in the structure, thereby causing initial irreversible effects, this behavior is very pronounced in the anatase TiO_2 nanotubes studied here and may be associated with the particularly large surface area of the nanotubes, which might interrupt a complete Li extraction. There are, however, additional effects to be considered, i.e. interstitial water in our $TiO_2{\cdot}0.18H_2O$ nanotubes and SEI formation. The irreversible capacity in the first discharge cycle might be affected by the decomposition of water molecules, which may be reduced to LiOH and Li_2O at low voltages and which may influence the amount of Li intercalated, especially in the first cycle.[27,35] Indeed, the water molecules seem to be completely consumed during the first discharge cycle, since by additional cycling no irreversible capacity was detected. This is reflected by the high Coulombic efficiency after the initial cycle (cf. Figure 6).

CONCLUSIONS

In summary, we report the synthesis of anatase and minor TiO_2(B) phase nanotubes by a hydrothermal process followed by heat treatment at 500 °C in argon for 1 h. The size of TiO_2 nanotubes is found to be about 4−6 nm in inner diameter and 10−15 nm in outer diameter, and the length up to 150 nm. The discharge capacity keeps 265 mAh/g after 50 galvanostatic cycles, presenting good cycling performance compared to other TiO_2 forms. The Coulombic efficiency of about 99% after cycle 50 implies excellent cycling stability. The good cyclability and a high-rate capability of nontoxic TiO_2 nanotubes prepared by a comparably simple method renders the material attractive for lithium-ion batteries aiming at high stability, lifetime, cost-efficiency, and safety.

AUTHOR INFORMATION

Corresponding Author

*E-mail: r.klingeler@kip.uni-heidelberg.de.

Notes

The authors declare no competing financial interest.

ACKNOWLEDGMENTS

A.P., C.J., and R.K. acknowledge support by Bundesministerium für Bildung und Forschung via the LIB2015 alliance (Independent research group 03SF0340/03SF0397). G.S.Z. acknowledges support by the DFG within project KL 1824/4.

REFERENCES

(1) Yahya, N., *Carbon and Oxide Nanostructures: Synthesis, Characteristic and Application*; Springer Verlag: Berlin, Heidelberg, 2011.
(2) Umar, A., Hahn, Y., Eds. *Metal Oxide Nanostructures and Their Applications*; American Scientific Publishers: Valencia, CA, 2010.
(3) Zakharova, G. S.; Volkov, V. L.; Ivanovskaya, V. V.; Ivanovskii, A. A. *Usp. Khim.* **2005**, *74*, 651−685.
(4) Chen, X.; Mao, S. S. *Chem. Rev.* **2007**, *107*, 2891−2959.
(5) Meekins, B. H.; Kamat, P. V. *ACS Nano* **2009**, *3*, 3437−3446.
(6) Armstrong, G.; Armstrong, A. R.; Canalas, J.; Garcia, R.; Bruce, P. G. *Electrochem. Solid State Lett.* **2006**, *9*, A139−A143.
(7) Ortiz, G. F.; Hanzu, I.; Djenizian, T.; Lavela, P.; Tirado, J. L.; Knauth, P. *Chem. Mater.* **2009**, *21*, 63−67.
(8) Zhang, H.; Li, G. R.; An, L. P.; Yan, T. Y.; Gao, X. P.; Zhu, H. Y. *J. Phys. Chem. C* **2007**, *111*, 6143−6148.
(9) Bavykin, D. V.; Friedrich, J. M.; Walsh, F. C. *Adv. Mater.* **2006**, *18*, 2807−2824.
(10) Dambournet, D.; Belharouak, I.; Amine, K. *Chem. Mater.* **2010**, *22*, 1173−1179.
(11) Jiang, C.; Wei, M.; Qi, Z.; Kudo, T.; Honmaa, I.; Zhou, H. *J. Power Sources* **2007**, *166*, 239−243.
(12) Peng, H.; Wang, X.; Li, G.; Pang, H.; Chen, X. *Mater. Lett.* **2010**, *64*, 1898−1901.
(13) Kasuga, T.; Hiramatsu, M.; Hoson, A.; Sekino, T.; Niihara, K. *Langmuir* **1998**, *14*, 3160−3163.
(14) (a) Popa, A. I.; Vavilova, E.; Täschner, C.; Kataev, V.; Büchner, B.; Klingeler, R. *J. Phys. Chem. C* **2011**, *115*, 5265−5270. (b) Popa, A. I.; Vavilova, E.; Arango, Y. C.; Täschner, C.; Kataev, V.; Klauss, H.-H.; Maeter, H.; Luetkens, H.; Büchner, B.; Klingeler, R. *Eur. Phys. Lett.* **2009**, *88*, 57002.
(15) Ma, R.; Bando, Y.; Sasaki, T. *Chem. Phys. Lett.* **2003**, *380*, 577−582.
(16) Feist, T. P.; Davies, P. K. *J. Solid State Chem.* **1992**, *101*, 275−295.
(17) Bavykin, D. V.; Friedrich, J. M.; Walsh, F. C. *Adv. Mater.* **2006**, *18*, 2807−2824.
(18) (a) Patterson, A. L. *Phys. Rev. Lett.* **1939**, *56*, 978−982. (b) El-Gendy, A. A.; Khavrus, O. V.; Hampel, S.; Leonhardt, A.; Büchner, B.; Klingeler, R. *J. Phys. Chem. C* **2010**, *114*, 10745−10749.
(19) Nakamura, R.; Imanishi, A.; Murakoshi, K.; Nakato, Y. *J. Am. Chem. Soc.* **2003**, *125*, 7443−7450.
(20) Li, S.; Ye, G.; Chen, G. *J. Phys. Chem.* **2009**, *113*, 4031−4037.
(21) Borghols, W. J. H.; Lützenkirchen-Hecht, D.; Haake, U.; Chan, W.; Lafont, U.; Kelder, E. M.; van Eck, E. R. H.; Kentgens, A. P. M.; Mulder, F. M.; Wagemaker, M. *J. Electrochem. Soc.* **2010**, *157*, A582−A588.
(22) Reddy, M. V.; Jose, R.; Teng, T. H.; Chowdari, B. V. R.; Ramakrishna, S. *Electrochim. Acta* **2010**, *55*, 3109−3117.
(23) Ye, J.; Liu, W.; Cai, J.; Chen, S.; Zhao, X.; Zhou, H.; Qi, L. *J. Am. Chem. Soc.* **2011**, *133*, 933−940.
(24) Cava, R. J.; Murphy, D. W.; Zahurak, S.; Santoro, A.; Roth, R. S. *J. Solid State Chem.* **1984**, *53*, 64−75.

(25) Wagemaker, M.; Kearley, G. J.; van Well, A. A.; Mutka, H.; Mulder, F. M. *J. Am. Chem. Soc.* **2003**, *125*, 840−848.
(26) Hu, Y.-S.; Kienle, L.; Guo, Y.-G.; Maier. *J. Adv. Mater.* **2006**, *18*, 1421−1426.
(27) Kim, J.; Cho, J. *J. Electrochem. Soc.* **2007**, *154*, A542−A564.
(28) Das, S. K.; Bhattacharyya, A. J. *J. Phys. Chem. C* **2009**, *113*, 17367−17371.
(29) Das, S. K.; Bhattacharyya, A. J. *J. Electrochem. Soc.* **2011**, *158*, A705−A710.
(30) Kavan, L.; Rathousky, J.; Grätzel, M.; Shklover, V.; Zukal, A. *J. Phys. Chem. B* **2000**, *104*, 12012−12020.
(31) Kavan, L.; Kalbác, M.; Zukalova, M.; Exnar, I.; Lorenzen, V.; Nesper, R.; Grätzel, M. *Chem. Mater.* **2004**, *16*, 477−485.
(32) Zukalova, M.; Kalbac, M.; Kavan, L.; Exnar, I.; Grätzel, M. *Chem. Mater.* **2005**, *17*, 1248−1255.
(33) Sudant, G.; Baudrin, E.; Larcher, D.; Tarascon, J.-M. *J. Mater. Chem.* **2005**, *15*, 1263−1269.
(34) Zhou, Y.-K.; Cao, L.; Zhang, F.-B.; He, B.-L.; Liz, H.-L. *J. Electrochem. Soc.* **2003**, *150*, A1246−A1249.
(35) Xu, J.; Jia, C.; Cao, B.; Zhang, W. F. *Electrochim. Acta* **2007**, *52*, 8044−8047.